




# Synthesis and characterization of single-phase epitaxial Cr<sub>2</sub>N thin films by reactive magnetron sputtering

M. A. Gharavi<sup>1,\*</sup> , G. Greczynski<sup>1</sup>, F. Eriksson<sup>1</sup>, J. Lu<sup>1</sup>, B. Balke<sup>2</sup>, D. Fournier<sup>3</sup>, A. le Febvrier<sup>1</sup>, C. Pallier<sup>1</sup>, and P. Eklund<sup>1</sup>

<sup>1</sup>Thin Film Physics Division, Department of Physics, Chemistry and Biology (IFM), Linköping University, 581 83 Linköping, Sweden

<sup>2</sup>Universität Stuttgart, Institut für Materialwissenschaft - Chemische Materialsynthese, Heisenbergstr. 3, 70569 Stuttgart, Germany

<sup>3</sup>UMR 7588, Institut des NanoSciences de Paris, CNRS, Sorbonne Université, 4 Place Jussieu, 75005 Paris, France

Received: 7 July 2018

Accepted: 8 September 2018

Published online:

18 September 2018

© The Author(s) 2018

## ABSTRACT

Cr<sub>2</sub>N is commonly found as a minority phase or inclusion in stainless steel, CrN-based hard coatings, etc. However, studies on phase-pure material for characterization of fundamental properties are limited. Here, Cr<sub>2</sub>N thin films were deposited by reactive magnetron sputtering onto (0001) sapphire substrates. X-ray diffraction and pole figure texture analysis show Cr<sub>2</sub>N (0001) epitaxial growth. Scanning electron microscopy imaging shows a smooth surface, while transmission electron microscopy and X-ray reflectivity show a uniform and dense film with a density of 6.6 g cm<sup>-3</sup>, which is comparable to theoretical bulk values. Annealing the films in air at 400 °C for 96 h shows little signs of oxidation. Nano-indentation shows an elastic–plastic behavior with  $H = 18.9$  GPa and  $E_r = 265$  GPa. The moderate thermal conductivity is 12 W m<sup>-1</sup> K<sup>-1</sup>, and the electrical resistivity is 70 μΩ cm. This combination of properties means that Cr<sub>2</sub>N may be of interest in applications such as protective coatings, diffusion barriers, capping layers and contact materials.

## Introduction

Chromium nitride (CrN) is a hard and corrosion resistant, semiconducting compound that has gained interest for various applications such as medical implants [1], silver luster decorative coatings [2], and wear-resistant coatings for cutting tools, especially when hot corrosion resistance is needed [3, 4]. It also has intriguing thermal and thermoelectric properties

[5–8]. Chromium nitride is an interstitial compound, in which nitrogen atoms reside in the octahedral spaces between the chromium atoms in an fcc lattice (i.e., rock-salt cubic), making the compound susceptible to stoichiometry deficiency. This leads to a second interstitial compound: metallic dichromium nitride (Cr<sub>2</sub>N). Both phases have a silver luster when seen by the naked eye and can be used as decorative coatings. Unlike CrN however, Cr<sub>2</sub>N crystallizes in a

Address correspondence to E-mail: mohammad.amin.gharavi@liu.se

hexagonal crystal structure and is usually reported as a secondary phase in either CrN hard coatings or steel [9–11]. Phase shifts between CrN and Cr<sub>2</sub>N have also been studied and are controlled by the partial pressure of nitrogen gas flow and deposition temperature [12]. In a previous paper [13] focused on monochromium nitride, we studied CrN thin films for its thermoelectric properties. These films were synthesized by reactive magnetron sputtering, and it was found that by decreasing the nitrogen content of the N<sub>2</sub>/Ar gas flow mixture, Cr<sub>2</sub>N nanoinclusions will form inside the CrN matrix. At a sufficiently low N<sub>2</sub>/Ar ratio, single-phase Cr<sub>2</sub>N could be synthesized. Thermoelectric measurements showed that Cr<sub>2</sub>N has a Seebeck coefficient of a few  $\mu\text{V K}^{-1}$ . Also, the electrical resistivity slightly increases from 56  $\mu\Omega\text{ cm}$  at room temperature up to 89  $\mu\Omega\text{ cm}$  at 750 K, showing that Cr<sub>2</sub>N is metallic in nature.

Yan and Chen [14] used first principles calculations to predict a Young's modulus of 356 GPa, suitable for hard-coating applications. This is due to the distance between N atom sites which are repulsive in nature, leading to enhanced stability of Cr<sub>2</sub>N. Wei et al. [15] reported higher hardness properties for mixed phase CrN/Cr<sub>2</sub>N films compared to single-phase CrN. Single-phase Cr<sub>2</sub>N has also been studied [16, 17] for its mechanical properties. However, these films either are polycrystalline or have small amounts of Cr impurities. Additional research on the synthesis of polycrystalline CrN/Cr<sub>2</sub>N alloys [18] or CrN/Cr<sub>2</sub>N multilayers [19, 20] shows promising results for the wood cutting industry due to their suitable adhesion, wear resistance and hardness of approximately 22 GPa coupled with a relative low price in comparison with diamond or even titanium-based coatings.

In the present paper, we report on synthesis and property characterization of single-phase, epitaxial Cr<sub>2</sub>N. These films were deposited by reactive magnetron sputtering, did not show any phase impurities and are single crystal.

## Experimental details

The deposition process was carried out by reactive dc magnetron sputtering in a high vacuum chamber (base pressure:  $3.0 \times 10^{-7}$  mbar at deposition temperature). Details of the deposition setup can be found elsewhere [21]. The films were deposited onto

(0001) sapphire substrates ( $10 \times 10 \times 0.5\text{ mm}^3$ , ultrasonically cleaned in hellmanex (3 min), de-ionized water, acetone and ethanol (10 min each) and blown dry using N<sub>2</sub> [22]). The substrates were heated 700 °C for 1 h prior to the deposition process and maintained until the end of the process. The films were deposited using a 7.5-cm Cr (Kurt J. Lesker, 99.95% pure) target and an argon/nitrogen gas mixture (99.9997% pure for both gases). The target power for chromium was kept constant and set at 60 W under a constant deposition pressure of 0.6 Pa (4.5 mTorr). The substrate holder was rotated with a speed of 17 rpm and was grounded. The deposition time was 120 min for the 17% nitrogen gas mixture (9 sccm N<sub>2</sub>, 45 sccm Ar).

X-ray diffraction (XRD)  $\theta$ - $2\theta$  scans were carried out in a PANalytical X'Pert PRO diffractometer system equipped with a Cu K $\alpha$  source operated at 45 kV and 40 mA. The incident optics was a Bragg–Brentano module including a 0.5° divergence slit and a 0.5° anti-scatter slit, and the diffracted optics included a 5.0-mm anti-scatter slit and 0.04-rad soller slits. The PreFIX detector was set to one-dimensional scanning line mode. Step sizes and collection times per step were 0.004° and 2 s, respectively. High-resolution XRD and pole figure measurements were performed in a PANalytical EMPYREAN diffractometer operated at 45 kV and 40 mA. For HRXRD (line focus mode), the incident optics was a hybrid monochromator 2 bounce Ge (220) module including a 0.5° divergence slit, and the diffracted optics was a 3 bounce Ge (220) symmetrical analyzer. The XRD step sizes and collection times per step were 0.001° and 0.8 s, respectively. For the pole figure measurements (point focus mode), a  $2 \times 2\text{ mm}^2$  crossed slit X-ray lens and a parallel plate collimator as the incident and diffracted beam optics were used, respectively. Pole figures of the Cr<sub>2</sub>N (0002) and ( $\bar{1}\bar{1}21$ ) peaks were acquired in the tilt-angle ( $\psi$ ) range between 0 and 85° and azimuth-angle ( $\varphi$ ) range between 0 and 360° with steps of 5° for both  $\psi$  and  $\varphi$  and a collection time of 1 s.

The chemical composition of the Cr<sub>2</sub>N films is deduced from X-ray photoelectron spectroscopy (XPS, Axis Ultra DLD, Kratos Analytical, UK) equipped with a monochromatic Al(K $\alpha$ ) X-ray radiation ( $h\nu = 1486.6\text{ eV}$ ) source. The base pressure in the analysis chamber during acquisition was less than  $1 \times 10^{-9}$  mbar. Survey spectra as well as XPS core

level spectra of the Cr 2p, N 1s and O 1s regions were recorded on as-deposited samples and after sputter cleaning for 600 s with a 0.5 keV Ar<sup>+</sup> ion beam carried out to remove the surface oxygen layer that grows upon air exposure. The Ar<sup>+</sup> beam had an incidence angle of 20° and was rastered over an area of 3 × 3 mm<sup>2</sup>. The core level spectra recorded after Ar<sup>+</sup> etching were used to extract the chemical composition of the CrN coatings. Here, a Shirley-type background was subtracted, and elemental cross sections provided by Kratos Analytical were applied. Due to preferential sputtering of nitrogen, a 3% error bar is expected [23]. XPS sputter depth profiles in 0.8 nm steps were also performed on samples annealed in air to evaluate resistance toward oxidation. In this case, the Ar<sup>+</sup> ion energy was 0.5 keV. Oxidation resistance testing was performed by heating a Cr<sub>2</sub>N thin film (epitaxial CrN and polycrystalline CrN thin films were included as reference samples) on a standard laboratory hot plate at 400 °C for 96 h under atmospheric conditions. The hot-plate temperature was measured with a thermocouple connected to a multimeter.

A JEOL 2200FS operating at 200 kV was used for transmission electron microscopy (TEM), high-resolution TEM (HRTEM), and selected area electron diffraction (SAED). Cross-sectional samples for the TEM were prepared by mechanically polishing them down to 55 μm by hand. Ion milling was then applied using a Gatan Precision Ion Polishing System (PIPS) with a 5 keV Ar<sup>+</sup> ion beam angled at 8° of incidence relative to the sample surface for 2 h and 5° for 4 h. Once electron transparency was reached, a final ion milling step was applied with lower energy ion beams (2 keV) for 30 min.

Sample surface morphologies were obtained by a LEO 1550 Gemini scanning electron microscope (SEM). The acceleration voltage was set to 5 kV.

The electrical resistivity of all samples was obtained by measuring the sheet resistance of the films with a four-point-probe Jandel RM3000 station and multiplying the sheet resistance with the film thickness of approximately 450 nm (obtained from cross-sectional TEM imaging). Such measurements include a ± 10 nm error bar.

Temperature-dependent Hall carrier concentrations were determined on 5 × 5 mm<sup>2</sup> substrates using the IPM-HT Hall-900 K system (developed and constructed by Fraunhofer IPM in Freiburg, Germany) and includes a 10% error bar. Thermal

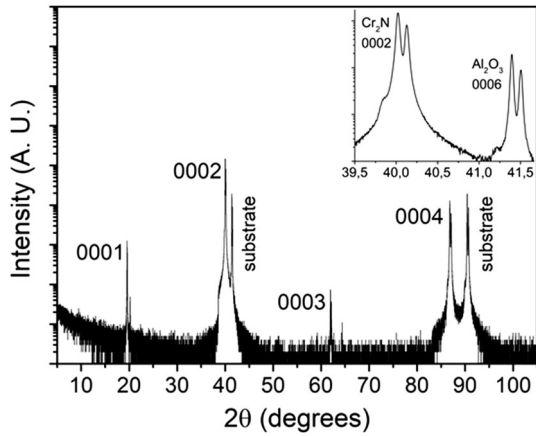
conductivity of selected samples was determined by modulated thermoreflectance microscopy (MTRM). In this setup, a pump beam at 532 nm (delivered by a Cobalt MLD laser and with the intensity modulated by an acousto-optical modulator at a frequency *f*) is focused on the surface of the sample with an objective lens (*N. A.* = 0.5). The samples were coated by a 100 nm gold layer, ensuring that the heat source is located at the surface. Thermal waves are excited in the sample and monitored by the reflectivity surface change recorded around the pump location by another focused laser beam. A 488 nm Oxixus laser is used to maximize the probe sensitivity toward the thermal field in the gold cap layer. A photodiode and a lock-in amplifier recorded the AC reflectivity component, in a frequency range between 1 kHz and 1 MHz. Finally, the experimental profiles of the amplitude and the phase of the reflected probe beam were fitted according to a standard Fourier diffusion law to extract the thermal conductivity of the films and include a measurement error of 15% [24–30].

The mechanical properties (hardness and elastic modulus) of the Cr<sub>2</sub>N films were investigated by nano-indentation using a Triboindenter TI 950 (Hysitron) and a Berkovich diamond tip with an apex radius of 100 nm. The mechanical response of the thin films was recorded for 30 nanoindents at a constrained load of 1300 μN in order to respect the rule of thumb of a maximal penetration depth below 10% of the film thickness. The data were analyzed using the approach of Oliver and Pharr [31].

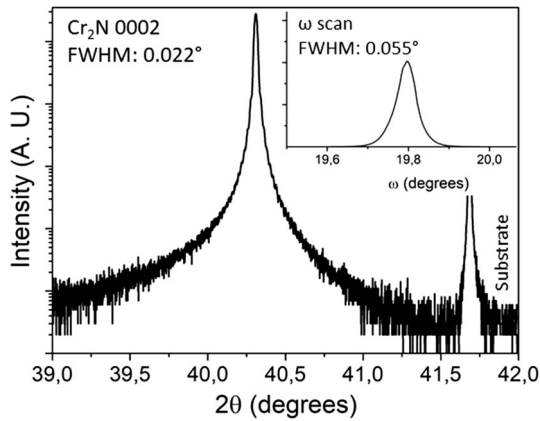
## Results

Figure 1 shows a  $\theta$ - $2\theta$  scan of Cr<sub>2</sub>N film on a *c*-cut sapphire substrate. Only peaks of the {0001} family are observed from the film, showing *c*-axis oriented growth. The inset is a close-up image of the Cr<sub>2</sub>N (0002) peak and the sapphire (0006) peak and shows  $K_{\alpha 1}$ - $K_{\alpha 2}$  peak splitting.

Figure 2 shows a high-resolution XRD scan of the Cr<sub>2</sub>N 0002 peak. The peak shows Laue oscillations (layer thickness fringes). The full width at half maximum (FWHM) is 0.022° compared to the FWHM value of 0.007° for the substrate peak. Rocking curve measurements of both the Cr<sub>2</sub>N 0002 (Fig. 2 inset) and 0004 peaks show FWHM values of 0.055° and 0.044°, respectively.



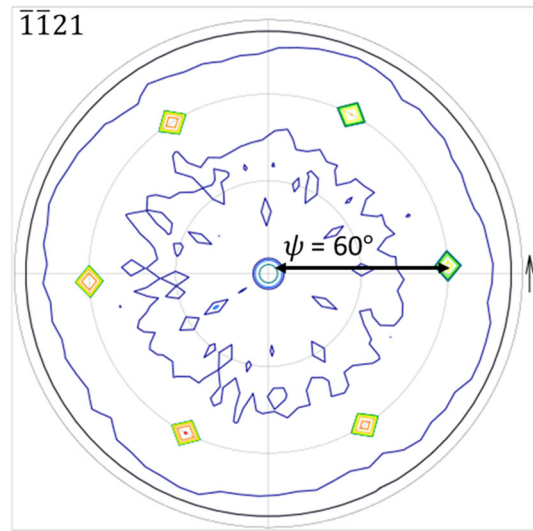
**Figure 1** XRD results of Cr<sub>2</sub>N deposited on sapphire substrates. Inset: close-up image of the Cr<sub>2</sub>N 0002 and Al<sub>2</sub>O<sub>3</sub> 0006 peaks. Note the  $K_{\alpha 1}$ – $K_{\alpha 2}$  peak splitting indicating high crystal quality.



**Figure 2** HRXRD measurement of Cr<sub>2</sub>N 0002 peak. Inset shows the rocking curve scan of Cr<sub>2</sub>N 0002.

Figure 3 shows a pole figure measurement of the Cr<sub>2</sub>N thin film. The pole figure is performed at  $2\theta = 42.76^\circ$  corresponding to the  $\bar{1}\bar{1}21$  peak. In this case, six high-intensity poles at  $\psi = 60^\circ$  surround a low-intensity pole in the center corresponding to the 0002 peak. Thus, a  $(1\bar{2}10)(0001)\text{Cr}_2\text{N}/(1\bar{2}10)(0001)\text{Al}_2\text{O}_3$  and  $[1\bar{1}00]\text{Cr}_2\text{N}/[1\bar{1}00]\text{Al}_2\text{O}_3$  epitaxial relationship leading to a single-crystal film on top of a single-crystal substrate is observed.

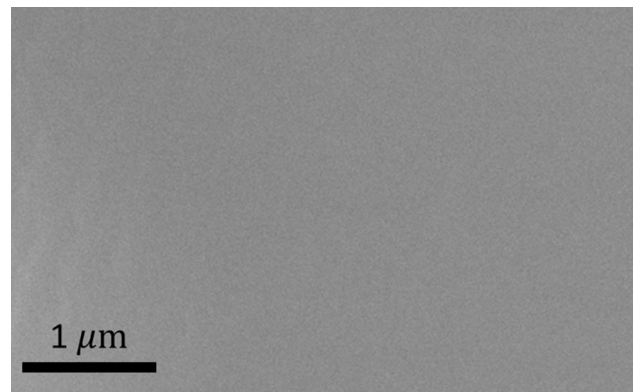
XPS measurements show that the Cr<sub>2</sub>N film is stoichiometric (Cr 2p = 69%, N 1s = 30%) and contain approximately 1% oxygen and a negligible amount of carbon. Figure 4 shows an SEM image of the film surface. The film surface is smooth and featureless, consistent with the observed epitaxial growth and the high surface diffusion at 700 °C (the deposition temperature).



**Figure 3** Pole figure texture analysis of Cr<sub>2</sub>N at  $2\theta = 42.76^\circ$  corresponding to the  $\bar{1}\bar{1}21$  peak.

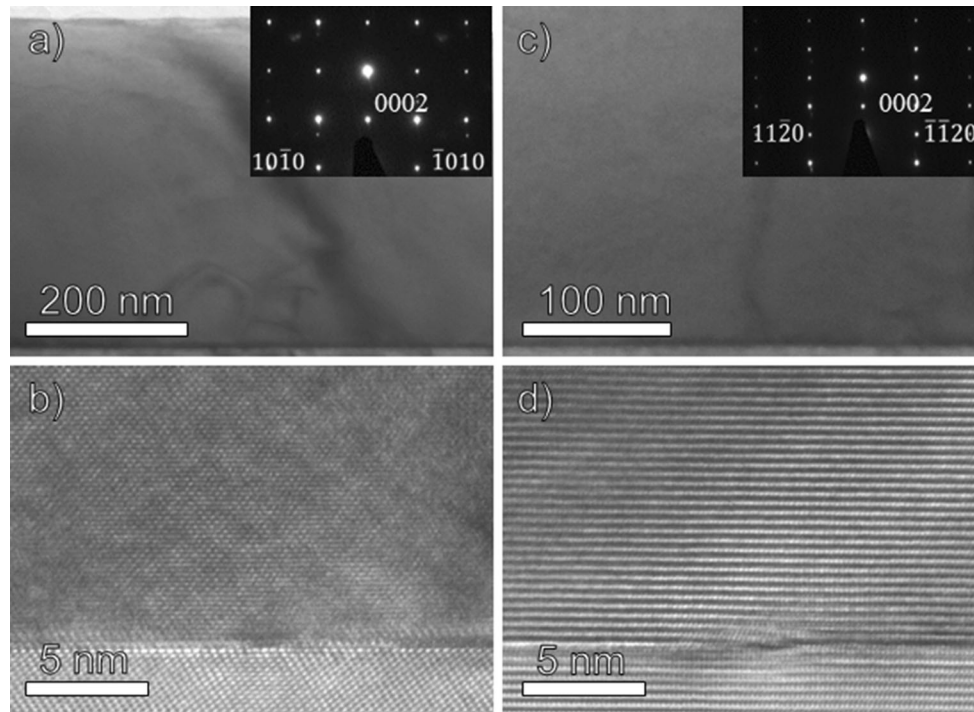
Figure 5 shows the TEM, HRTEM and SAED images for Cr<sub>2</sub>N. The images show a dense and single-crystal film with no grain boundaries in that scale. Epitaxy with the substrate is also seen which includes a sharp interface between film and substrate. In Fig. 5a, the TEM zone axis is in the  $[1\bar{2}10]$  direction, while in Fig. 5c, the TEM zone axis is in the  $[1\bar{1}00]$  direction.

Table 1 lists measured physical properties of the Cr<sub>2</sub>N film. According to the XRR measurements, the film has an arithmetic averaged roughness ( $R_a$ ) of 0.9 nm, which is comparable with polished, single-crystal substrates (0.5 nm). The same measurements also show a film density of  $6.6\text{ g cm}^{-3}$ , which is comparable to the theoretical bulk value of  $6.72\text{ g cm}^{-3}$  [32].



**Figure 4** SEM image of Cr<sub>2</sub>N surface.





**Figure 5** TEM, HRTEM and SAED images of  $\text{Cr}_2\text{N}$  showing a dense and single-crystal film. **a** and **b** TEM and HRTEM image of the film in the  $[\bar{1}210]$ -zone axis including total film thickness ( $\sim 450$  nm) and epitaxial relationship with substrate. **c** and **d**

TEM and HRTEM image of the film in the  $[\bar{1}100]$ -zone axis and epitaxial relationship with substrate. Note the layered structure of  $\text{Cr}_2\text{N}$  when viewed from the  $[\bar{1}100]$ -zone axis.

**Table 1** Collective data on the physical properties of  $\text{Cr}_2\text{N}$  including film density, roughness, stoichiometry, hardness, elastic modulus, electrical resistivity, thermal conductivity and charge carrier density

Sample phase and thickness	Hardness and elastic modulus (GPa)	XRR measurements: roughness and density		Room temp. resistivity ( $\mu\Omega$ cm)	Room temp. thermal conductivity ( $\text{W m}^{-1}\text{K}^{-1}$ )	Charge carrier concentration ( $\text{cm}^{-3}$ )	
		$R_a$ (nm)	Density ( $\text{g cm}^{-3}$ )			300 K	800 K
Hexagonal $\text{Cr}_2\text{N}$ $\sim 450$ nm	$H = 18.9 \pm 0.5$ $E_r = 265 \pm 6$	$0.9 \pm 0.1$	$6.6 \pm 0.5$	$70 \pm 7$	$12.0 \pm 1.8$	$8.17 \times 10^{22}$	$28.70 \times 10^{22}$

Room temperature in-plane electrical resistivity is measured to be  $70 \mu\Omega$  cm. This value is an average of four samples, with four measurements performed on each sample. The standard deviation in these measurements is  $0.5 \mu\Omega$  cm. Hall coefficient measurements show the concentration of charge carriers to be  $8 \times 10^{22}$  and  $29 \times 10^{22} \text{ cm}^{-3}$  at room temperature and 800 K, respectively. The room temperature in-plane thermal conductivity measurement is measured to be  $12.0 \text{ W m}^{-1} \text{ K}^{-1}$ , which is relatively low for metals and comparable to elemental mercury (8.4

$\text{W m}^{-1} \text{ K}^{-1}$ ) or nichrome alloys (between 10 and  $20 \text{ W m}^{-1} \text{ K}^{-1}$  depending on alloy composition) [33, 34]. However, this value is three to four times larger than semiconducting CrN thin films [13].

Figure 6 shows the load versus displacement results for the nano-indentation measurement. Epitaxial  $\text{Cr}_2\text{N}$  shows a semi elastic–plastic behavior due to the 25 nm displacement in the tip position before and after the load. The hardness and reduced elastic modulus of the film are  $H = 18.9 \pm 0.5$  GPa and  $E_r = 265 \pm 6$  GPa, respectively. The error bar is based

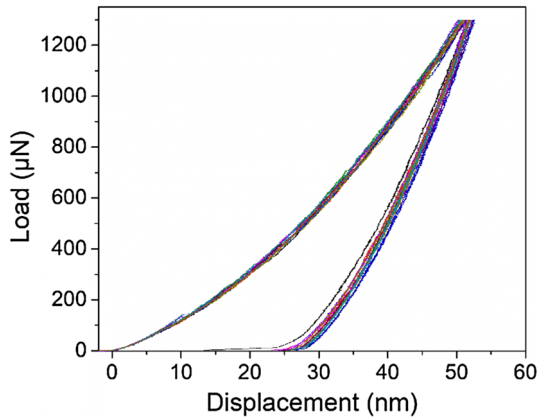


**Figure 6** XPS results for the 400 °C oxidation test. Epitaxial CrN and epitaxial Cr<sub>2</sub>N were heated for 96 h, while as polycrystalline CrN was only heated for 48 h.

on the standard deviation in 28 measurements. In comparison, the hardness and reduced elastic modulus of titanium nitride (TiN) are  $H = 20.0 \pm 0.8$  GPa and  $E_r = 445 \pm 38$  GPa, respectively [35].

Figure 7 shows the O concentration obtained from XPS sputter depth profiles performed in order to test the oxidation resistance during annealing in air for epitaxial Cr<sub>2</sub>N, epitaxial CrN and compare it to that of polycrystalline CrN used here as a reference sample. Epitaxial CrN [13] and epitaxial Cr<sub>2</sub>N were heated at 400 °C for 96 h, while the polycrystalline CrN test sample [36] was only heated for 48 h. XPS results reveal that in the case of epitaxial films the elevated oxygen concentration persists down to the depth of 8 nm from the surface, after which the signal saturates at the level of 1.3 at % which is due to residual O atoms implanted during the Ar<sup>+</sup>-etching

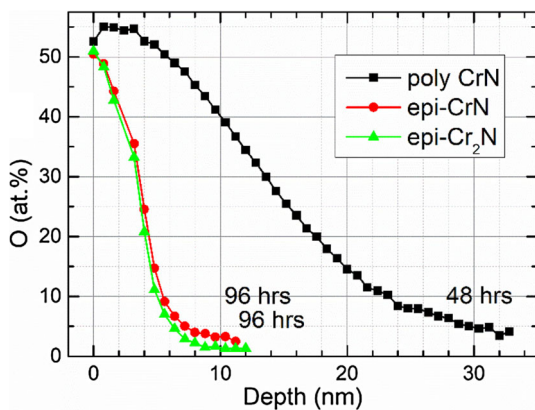


**Figure 7** Load versus displacement plot for hardness measurements on Cr<sub>2</sub>N. The film shows an elastic–plastic behavior.

process. In contrast, the polycrystalline CrN film exhibits higher O content even after removing first 30 nm from the surface and essentially never reaches the purity observed for the epitaxial films.

### Discussions

In general, all measurements indicate that Cr<sub>2</sub>N has been synthesized in the form of a dense, single-phase and single-crystal film.  $K_{\alpha 1}$ – $K_{\alpha 2}$  peak splitting in the low-resolution XRD measurements are visible in both film and substrate peaks indicating high crystal quality due to the minor energy difference between the  $K_{\alpha 1}$ – $K_{\alpha 2}$  X-rays, which would not be resolved for lower crystal quality. The HRXRD measurements show Laue oscillations (layer thickness fringes) which are only seen in very smooth films [37]. By using the equation  $t = \frac{\lambda(n_2 - n_1)}{2(\sin \theta_2 - \sin \theta_1)}$  for two consecutive fringes, film thickness can be calculated where  $t$  is film thickness,  $\lambda$  is the X-ray wavelength,  $\theta$  is the diffraction angle of the fringe and  $n$  is the fringe number. In our case, film thickness is calculated to be approximately 470 nm. The rocking curve measurements on the (0002) and (0004) peaks have similar full width at half maximum values, indicating little to no mosaicity in the film growth. This is because misaligned crystallites would broaden the rocking curve measurement. Pole figure measurements also show discrete poles which contrasts pole figure rings seen in polycrystalline films [37]. Due to the very low lattice mismatch between Cr<sub>2</sub>N [38] and Al<sub>2</sub>O<sub>3</sub> [39], an overlap between the a-axis and b-axis of Cr<sub>2</sub>N and Al<sub>2</sub>O<sub>3</sub> leads to a featureless film as seen in the SEM image (Fig. 4). The TEM and HRTEM images (Fig. 5) show the film to be single crystal, and the XRR measurements show that the film density is close to theoretical bulk crystal values, which is expected for a single-crystal film.

Although the electrical resistivity and charge carrier concentrations of Cr<sub>2</sub>N are similar to a metal, thermal conductivity measurements show a relatively low value of 12.0 W m<sup>-1</sup> K<sup>-1</sup> (Table 1). In comparison, the thermal conductivity of semiconducting CrN is approximately 4.0 W m<sup>-1</sup> K<sup>-1</sup>, while this value for insulating sapphire is approximately 30.0 W m<sup>-1</sup> K<sup>-1</sup> [39]. According to the Wiedemann–Franz law, the product of the electrical resistivity and thermal conductivity is a constant:  $\rho\kappa = LT$ , where  $L$

is the Lorenz number ( $2.44 \times 10^{-8} \text{ W}\Omega \text{ K}^{-2}$ ) and  $T$  is temperature. For our case,  $LT/\rho = 10.5 \text{ Wm}^{-1}\text{K}^{-1}$ , thus proving that the phonon contribution in  $\text{Cr}_2\text{N}$  thermal conductivity is small compared to the electrical contribution (as is in other metals).

As for the oxidation test, the results show that after the annealing process, sputter cleaning of epitaxial  $\text{CrN}$  and epitaxial  $\text{Cr}_2\text{N}$  will remove an 8 nm oxide layer compared to the 30 nm oxide layer of polycrystalline  $\text{CrN}$  (and which was only annealed for half the time), thus proving the advantage of single-crystal films compared to that of polycrystalline ones where oxidation may proceed through grain boundaries. These features (plus the silver luster of the film) could be suitable for decorative hard coatings, contact material [40, 41], capping and diffusion layer [42, 43] applications or used as tough oxidation resistant films [44, 45] similar to other transition metal nitrides.

## Conclusions

Single-phase, epitaxial dichromium nitride thin films were synthesized by reactive magnetron sputter deposition onto c-cut sapphire substrates. These films are single crystal, permitting the characterization of the fundamental properties of this material system.  $\text{Cr}_2\text{N}$  is metallic with an electrical resistivity of  $70 \mu\Omega \text{ cm}$  at room temperature but a relatively low thermal conductivity value of  $12.0 \text{ W m}^{-1} \text{ K}^{-1}$ . These values are comparable with elements such as mercury or alloys such as nichrome.  $\text{Cr}_2\text{N}$  is shown to have an elastic–plastic behavior with a hardness and reduced elastic modulus of  $H = 18.9 \pm 0.5 \text{ GPa}$  and  $E_r = 265 \pm 6 \text{ GPa}$ , respectively, suitable for soft bearing surfaces. It is also oxidation resistant up to at least  $400 \text{ }^\circ\text{C}$  for 96 h. This, plus its silver luster, suggests  $\text{Cr}_2\text{N}$  thin films as an interesting material for decorative hard coatings, contact material, capping and diffusion layer applications.

## Acknowledgements

The authors acknowledge funding from the European Research Council under the European Community's Seventh Framework Programme (FP/2007-2013)/ERC Grant Agreement No. 335383, the Swedish Government Strategic Research Area in Materials

Science on Functional Materials at Linköping University (Faculty Grant SFO-Mat-LiU No. 2009 00971), the Swedish Foundation for Strategic Research (SSF) through the Future Research Leaders 5 program, The Knut and Alice Wallenberg foundation through the Wallenberg Academy Fellows program, and the Swedish Research Council (VR) under Project No 2016-03365. We also acknowledge the financial support from the Åforsk Foundation Grant 16-359, and Carl Tryggers Foundation Contract CTS 17:166.

## Compliance with ethical standards

**Conflict of interest** The authors declare that they have no conflict of interests.

**Open Access** This article is distributed under the terms of the Creative Commons Attribution 4.0 International License (<http://creativecommons.org/licenses/by/4.0/>), which permits unrestricted use, distribution, and reproduction in any medium, provided you give appropriate credit to the original author(s) and the source, provide a link to the Creative Commons license, and indicate if changes were made.

## References

- [1] Williams S, Tipper JL, Ingham E, Stone MH, Fisher J (2003) In vitro analysis of the wear, wear debris and biological activity of surface-engineered coatings for use in metal-on-metal total hip replacements. *Proc. Inst Mech. Eng* 217:155–163
- [2] Hones P, Martin N, Regula M, Lévy F (2003) Structural and mechanical properties of chromium nitride, molybdenum nitride, and tungsten nitride thin films. *J Phys D Appl Phys* 36:1023–1029
- [3] Swadźba L, Maciejny A, Formanek B, Liberski P, Podolski P, Mendala B, Gabriel H, Poznańska A (1996) Influence of coatings obtained by PVD on the properties of aircraft compressor blades. *Surf Coat Technol* 78:137–143
- [4] Panjan P, Navinšek B, Cvelbar A, Zalar A, Milošev I (1996) Oxidation of TiN, ZrN, TiZrN, CrN, TiCrN and TiN/CrN multilayer hard coatings reactively sputtered at low temperature. *Thin Solid Films* 282:298–301
- [5] Quintela CX, Rodríguez-González B, Rivadulla F (2014) Thermoelectric properties of heavy-element doped CrN. *Appl Phys Lett* 104:022103

- [6] Kerdsonpanya S, Sun B, Eriksson F, Jensen J, Lu J, Koh YK, Nong NV, Balke B, Alling B, Eklund P (2016) Experimental and theoretical investigation of  $\text{Cr}_{1-x}\text{Sc}_x\text{N}$  solid solutions for thermoelectrics. *J Appl Phys* 120:215103
- [7] Eklund P, Kerdsonpanya S, Alling B (2016) Transition-metal-nitride-based thin films as novel energy harvesting materials. *J Mater Chem C* 4:3905–3914
- [8] le Febvrier A, Nong NV, Abadias G, Eklund P (2018) P-type Al-doped Cr-deficient CrN thin films for thermoelectrics. *Appl Phys Express* 11:051003
- [9] Sanjinés R, Hones P, Lévy F (1998) Hexagonal nitride coatings: electronic and mechanical properties of  $\text{V}_2\text{N}$ ,  $\text{Cr}_2\text{N}$  and  $\delta\text{-MoN}$ . *Thin Solid Films* 332:225–229
- [10] Simmons JW, Atteridge DG, Rawers JC (1994) Sensitization of high-nitrogen austenitic stainless steels by dichromium nitride precipitation. *Corrosion* 7:491–501
- [11] Simmons JW, Covino BS Jr, Hawk JA, Dunning JS (1996) Effect of nitride ( $\text{Cr}_2\text{N}$ ) precipitation on the mechanical, corrosion, and wear properties of austenitic stainless steel. *ISIJ Int* 36:846–854
- [12] Hones P, Sanjines R, Levy F (1997) Characterization of sputter-deposited chromium nitride thin films for hard coatings. *Surf Coat Technol* 94–95:398–402
- [13] Gharavi MA, Kerdsonpanya S, Schmidt S, Eriksson F, Nong NV, Lu J, Balke B, Fournier D, Belliard L, le Febvrier A, Pallier C, Eklund P (2018) Microstructure and thermoelectric properties of CrN and CrN/ $\text{Cr}_2\text{N}$  thin films. *J Phys D Appl Phys* 51:355302
- [14] Yan MF, Chen HT (2014) Structural, elastic and electronic properties of  $\text{Cr}_2\text{N}$ : a first-principles study. *Comp. Mater. Sci.* 88:81–85
- [15] Wei G, Rar A, Barnard JA (2001) Composition, structure, and nanomechanical properties of DC-sputtered  $\text{CrN}_x$  ( $0 \leq x \leq 1$ ) thin films. *Thin Solid Films* 398–399:460–464
- [16] Lin J, Sproul WD, Moore JJ, Lee S, Myers S (2011) High rate deposition of thick CrN and  $\text{Cr}_2\text{N}$  coatings using modulated pulse power (MPP) magnetron sputtering. *Surf Coat Technol* 205:3226–3234
- [17] Wan P, Zhang Z, Holec D, Daniel R, Mitterer C, Duan H (2015) Nitrogen atom shift and the structural change in chromium nitride. *Acta Mater* 98:119–127
- [18] Djouadi MA, Nouveau C, Beer P, Lambertin M (2000)  $\text{Cr}_x\text{N}_y$  hard coatings deposited with PVD method on tools for wood machining. *Surf Coat Technol* 133–134:478–483
- [19] Aouadi SM, Schultze DM, Rohde SL, Wong K-C, Mitchell KAR (2001) Growth and characterization of  $\text{Cr}_2\text{N}/\text{CrN}$  multilayer coatings. *Surf Coat Technol* 140:269–277
- [20] Warcholinski B, Gilewicz A, Ratajski J (2011)  $\text{Cr}_2\text{N}/\text{CrN}$  multilayer coatings for wood machining tools. *Tribol Int* 44:1076–1082
- [21] Eriksson F, Johansson GA, Hertz HM, Birch J (2002) Enhanced soft x-ray reflectivity of Cr/Sc multilayers by ion-assisted sputter deposition. *Opt Eng* 41:2903–2909
- [22] Le Febvrier A, Jensen J, Eklund P (2017) Wet-cleaning of  $\text{MgO}(001)$ : modification of surface chemistry and effects on thin film growth investigated by x-ray photoelectron spectroscopy and time-of-flight secondary ion mass spectroscopy. *J Vac Sci Technol A* 35:021407
- [23] Haasch RT, Lee T-Y, Gall D, Greene JE, Petrov I (2000) Epitaxial  $\text{TiN}(001)$  grown and analyzed In situ by XPS and UPS. II. Analysis of  $\text{Ar}^+$  sputter etched layers. *Sur Sci Spec* 7:204–212
- [24] Pottier L (1994) Micrometer scale visualization of thermal waves by photoreflectance microscopy. *Appl Phys Lett* 64:1618–1619
- [25] Li B, Roger J-P, Pottier L, Fournier D (1999) Complete thermal characterization of film-on-substrate system by modulated thermoreflectance microscopy and multiparameter fitting. *J Appl Phys* 86:5314–5316
- [26] Plamann K, Fournier D, Forget BC, Boccara AC (1996) Microscopic measurements of the local heat conduction in polycrystalline diamond films. *Diam Relat Mater* 5:699–705
- [27] Frétigny C, Roger JP, Reita V, Fournier D (2007) Analytical inversion of photothermal measurements: independent determination of the thermal conductivity and diffusivity of a conductive layer deposited on an insulating substrate. *J Appl Phys* 102:116104
- [28] Frétigny C, Duquesne J-Y, Fournier D, Xu F (2012) Thermal insulating layer on a conducting substrate. Analysis of thermoreflectance experiments. *J Appl Phys* 111:084313
- [29] Xu F, Frétigny C, Fournier D, Belliard L, Vincent S, Perrin B, Martin S, Secouard C, Duquesne J-Y (2013) Lateral heat diffusion investigation of a layered structure: application to the complete thermal characterization of a lithium phosphorous oxynitride film. *J Appl Phys* 113:244304
- [30] Frétigny C, Duquesne J-Y, Fournier D (2015) Perturbation of the heat lateral diffusion by interface resistance in layered structures. *Int J Thermophys* 5–6:1281–1288
- [31] Oliver WC, Pharr GM (1992) An improved technique for determining hardness and elastic modulus using load and displacement sensing indentation experiments. *J Mater Res* 7(6):1564–1583
- [32] Jain A, Ong SP, Hautier G, Chen W, Richards WD, Dacek S, Cholia S, Gunter D, Skinner D, Ceder G, Persson KA (2013) Commentary: the materials project: a materials genome approach to accelerating materials innovation. *APL Mater* 1:011002
- [33] Powell RW, Ho CY, Liley CE (1966) Thermal conductivity of selected materials. U.S. Department of Commerce,



- National Standard Reference Data Series, National Bureau of Standards Publications, Washington
- [34] Endo R, Shima M, Susa M (2010) Thermal-conductivity measurements and predictions for Ni–Cr solid solution alloys. *Int J Thermophys* 31:1991–2003
- [35] Ljungcrantz H, Odén M, Hultman L, Greene JE, Sundgren J-E (1996) Nanoindentation studies of single-crystal (001)-, (011)-, and (111)-oriented TiN layers on MgO. *J Appl Phys* 80:6725–6733
- [36] Greczynski G, Jensen J, Böhlmark J, Hultman L (2010) Microstructure control of CrN<sub>x</sub> films during high power impulse magnetron sputtering. *Surf Coat Technol* 205:118–130
- [37] Birkholz M (2006) Thin film analysis by X-ray scattering. WILEY-VCH Verlag GmbH & Co, Weinheim
- [38] Kim SJ, Marquart T, Franzen HF (1990) Structure refinement for Cr<sub>2</sub>N. *J Less-Common Met* 158:L9–L10
- [39] Dobrovinskaya ER, Lytvynov LA, Pishchik V (2009) Sapphire: material, manufacturing, applications. Springer, Berlin
- [40] Luther BP, Mohny SE, Jackson TN (1998) Titanium and titanium nitride contacts to n-type gallium nitride. *Semicond Sci Technol* 13:1322–1327
- [41] Ren F, Abernathy CR, Chu SNG, Lothian JR, Pearton SJ (1995) Use of InN for ohmic contacts on GaAs/AlGaAs heterojunction bipolar transistors. *Appl Phys Lett* 66:1503–1505
- [42] Tsai MH, Sun SC, Tsai CE, Chuang SH, Chiu HT (1996) Comparison of the diffusion barrier properties of chemical-vapor-deposited TaN and sputtered TaN between Cu and Si. *J Appl Phys* 79:6932–6938
- [43] Becker JS, Gordon RG (2003) Diffusion barrier properties of tungsten nitride films grown by atomic layer deposition from bis(*tert*-butylimido)bis(dimethylamido)tungsten and ammonia. *Appl Phys Lett* 82:2239–2241
- [44] Chen Y, Zou J, Campbell SJ, Le Caer G (2004) Boron nitride nanotubes: pronounced resistance to oxidation. *Appl Phys Lett* 84:2430–2432
- [45] Chim YC, Ding XZ, Zeng XT, Zhang S (2009) Oxidation resistance of TiN, CrN, TiAlN and CrAlN coatings deposited by lateral rotating cathode arc. *Thin Solid Films* 517:4845–4849